

Dalton Transaction

2019

Electronic Supplementary Information (ESI)

**Experimental and Theoretical Investigation of Metalloreceptor
Bearing $[\text{Re}(\text{CO})_3]^+$ Core Incorporating Multifunctional Ligand:
Selective Reactivity Towards Zn^{2+} and CN^- Ion.**

Tapashi Das, Kajal Krishna Rajak*

*Inorganic Chemistry Section, Department of Chemistry, Jadavpur University, Kolkata,
700032, India.*

Email: kajalrajak@hotmail.com, kkrajak@chemistry.jdvu.ac.in

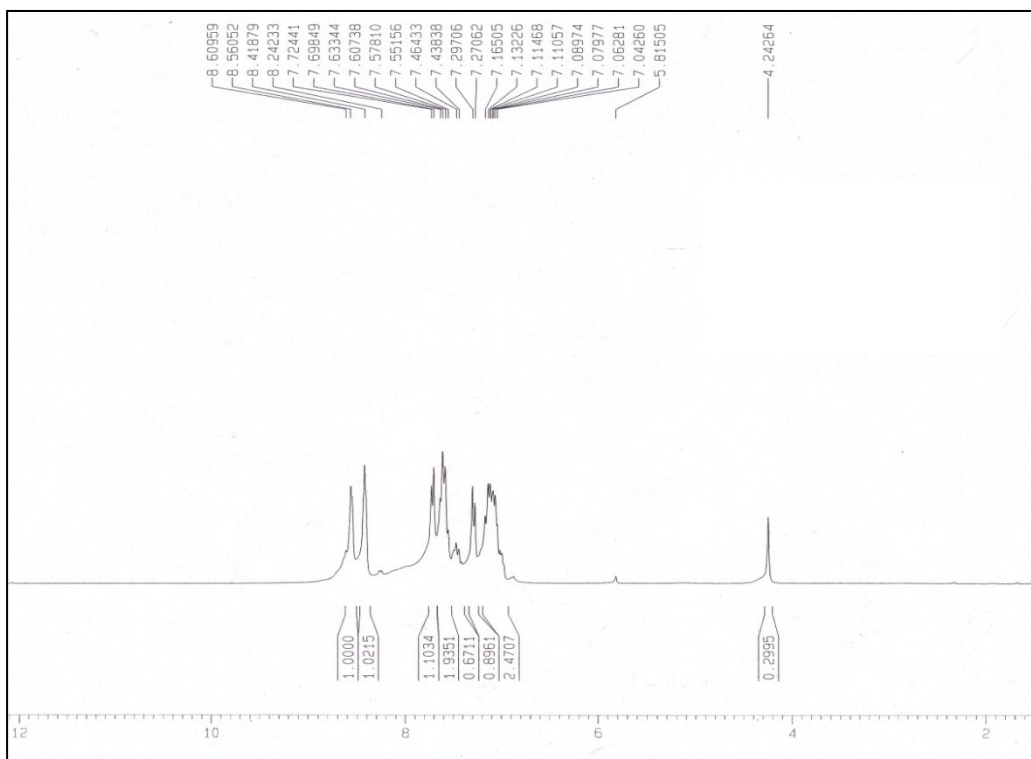


Figure-S1: ¹H NMR of 1st step (A) of ligand (HL)

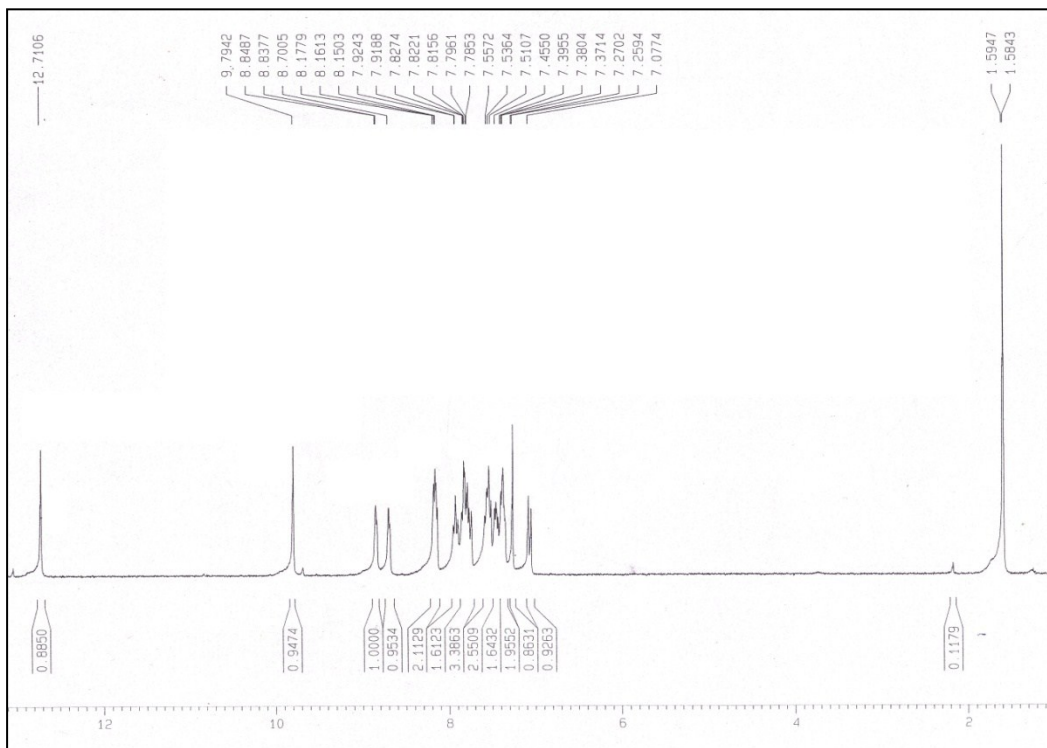


Figure-S2: ^1H NMR of Ligand (HL)

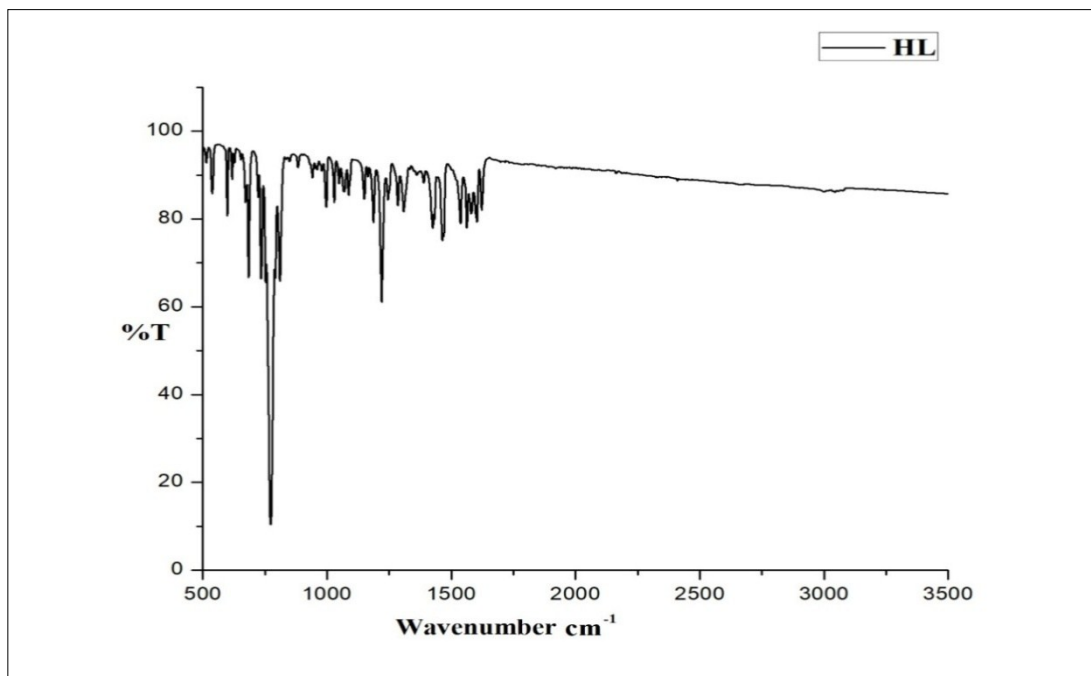


Figure-S3: IR spectra of ligand (HL)

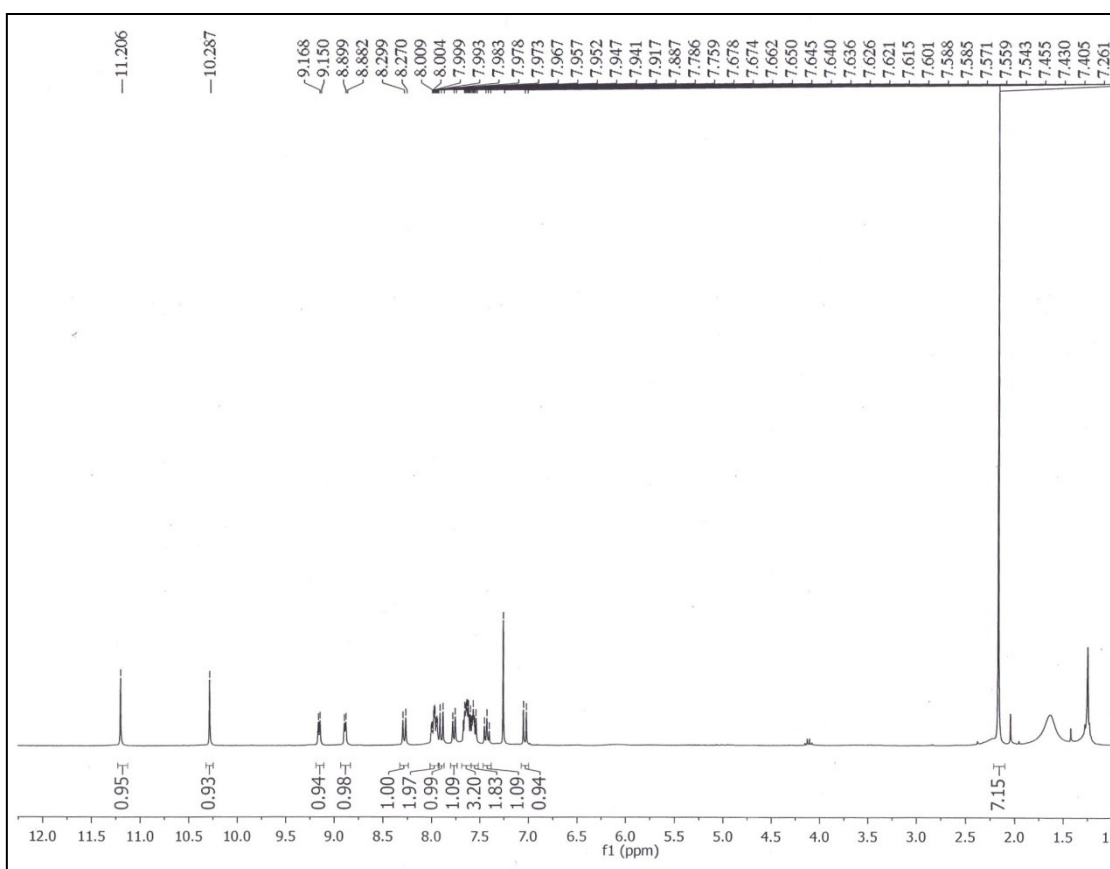


Figure-S4: ^1H NMR spectra of Complex 1

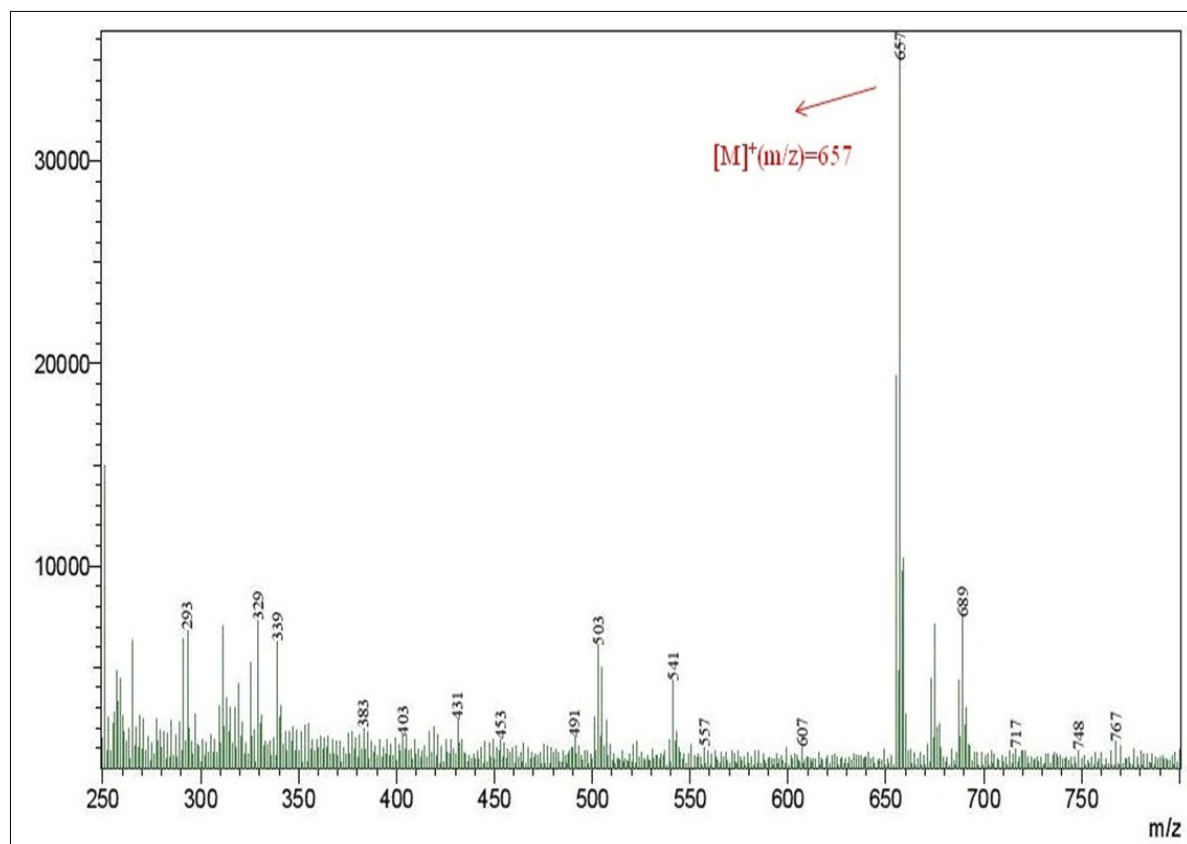


Figure-S5: Mass spectrum of Complex 1

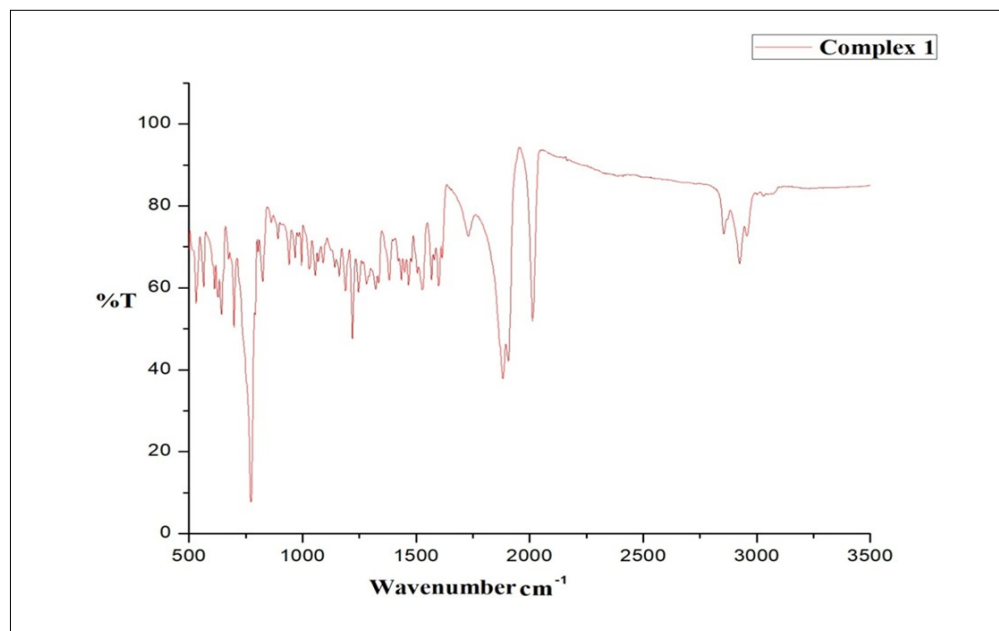


Figure-S6: IR spectra of Complex 1

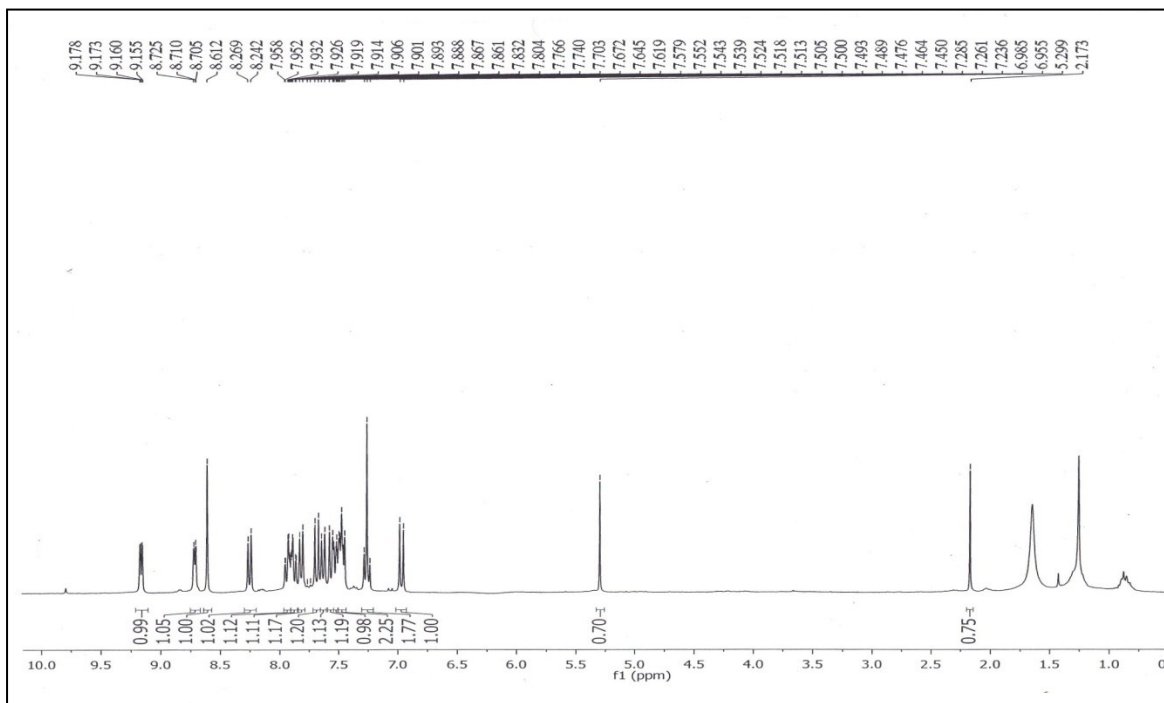


Figure-S7: ^1H NMR spectra of Complex 2

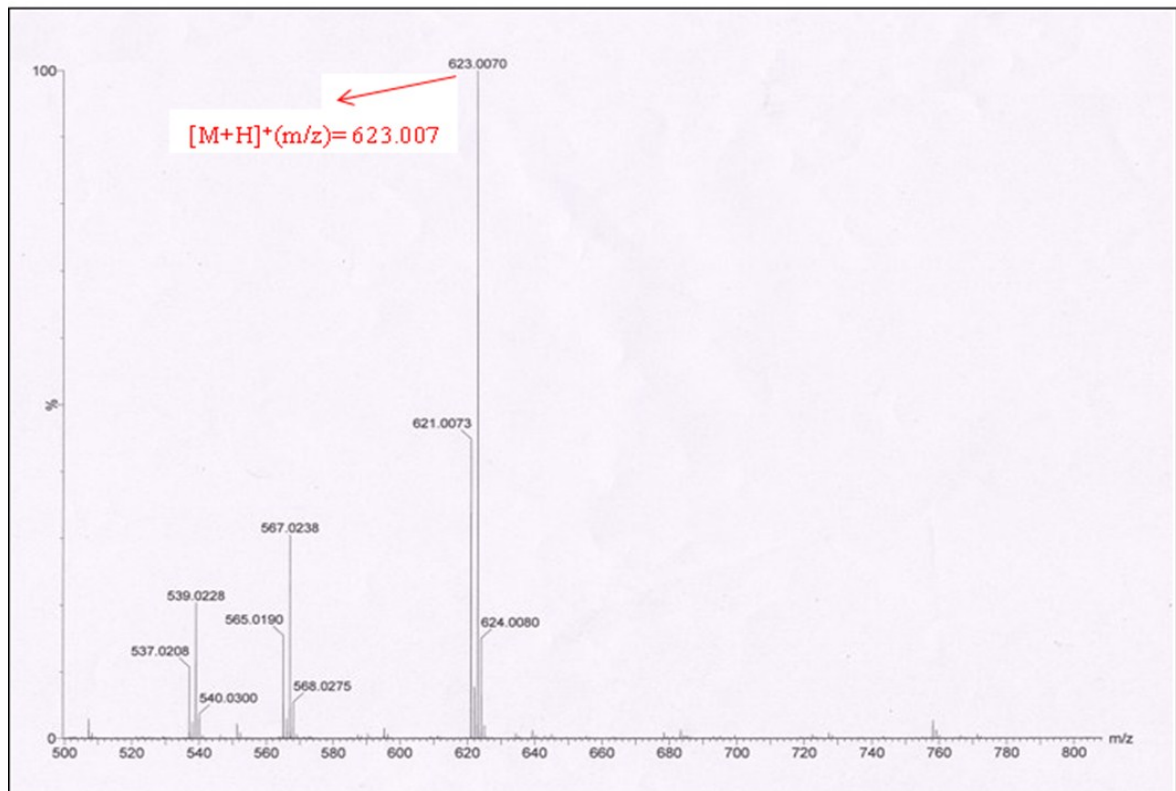


Figure-S8: Mass spectrum of Complex 2

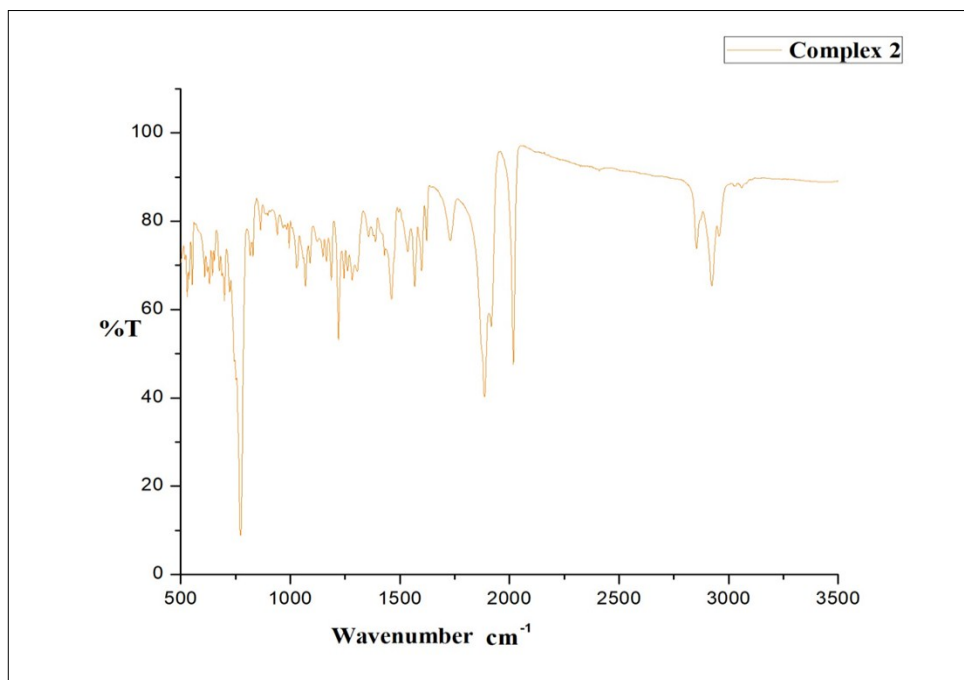


Figure-S9: IR spectra of Complex 2

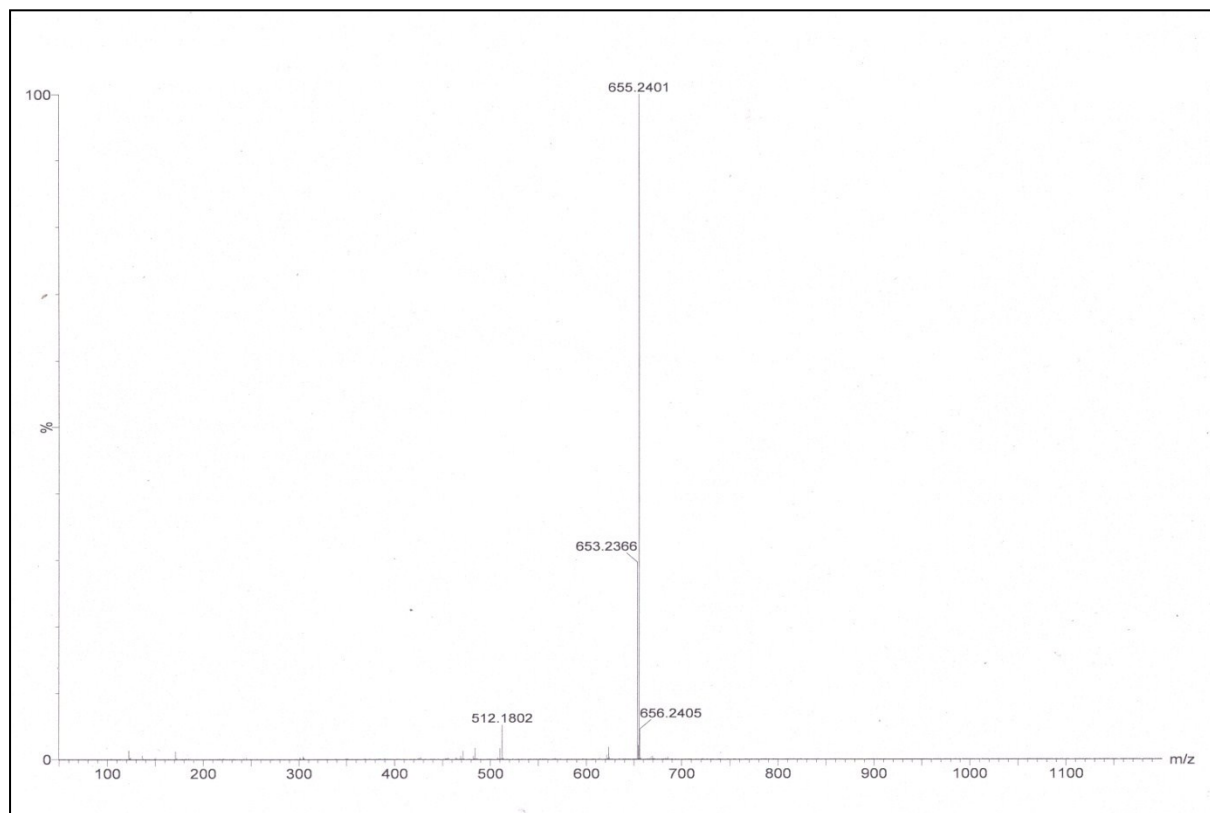


Figure-S10: Mass spectrum of Complex 3

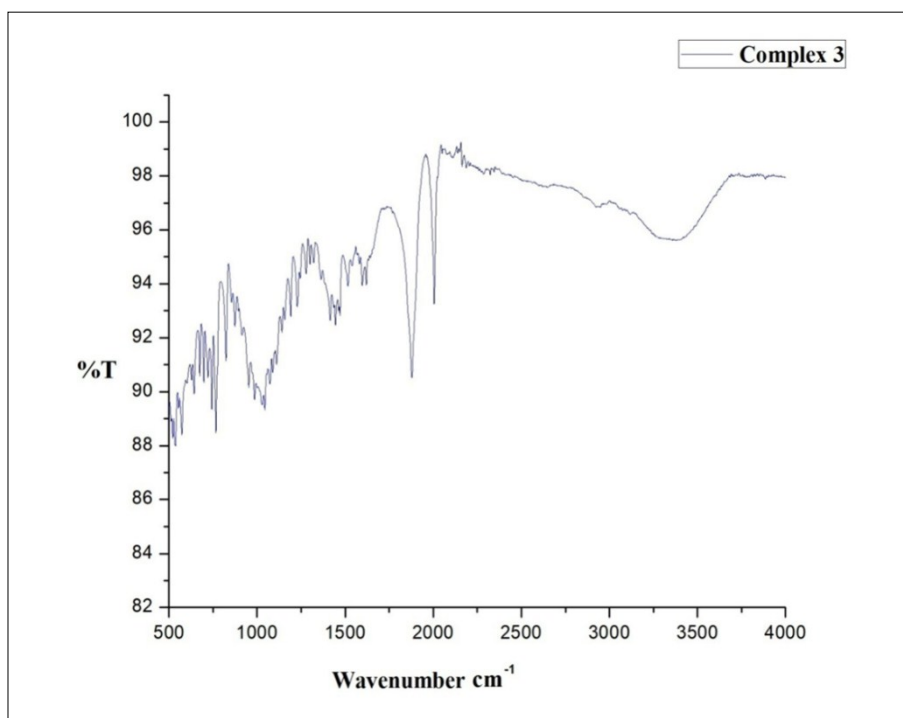


Figure-S11: IR spectra of Complex 3

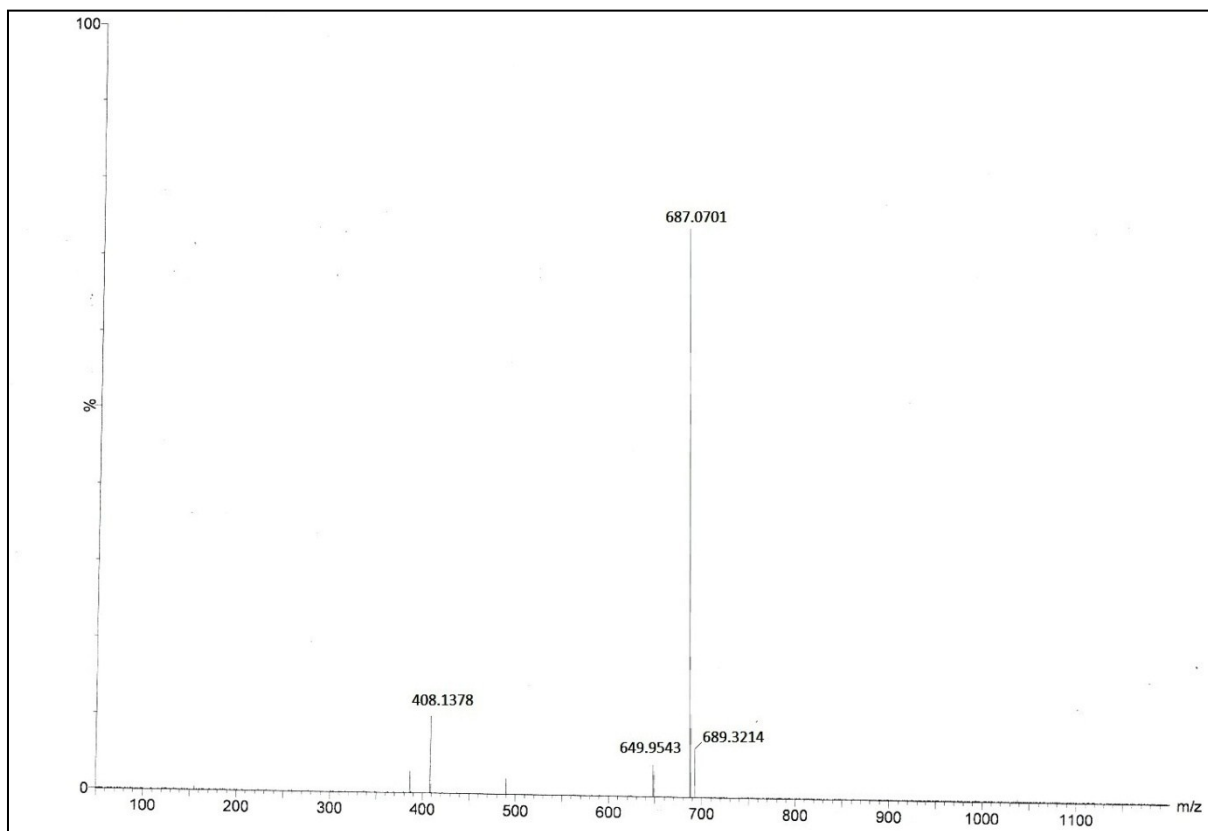


Figure-S12: Mass spectrum of cyanide adduct

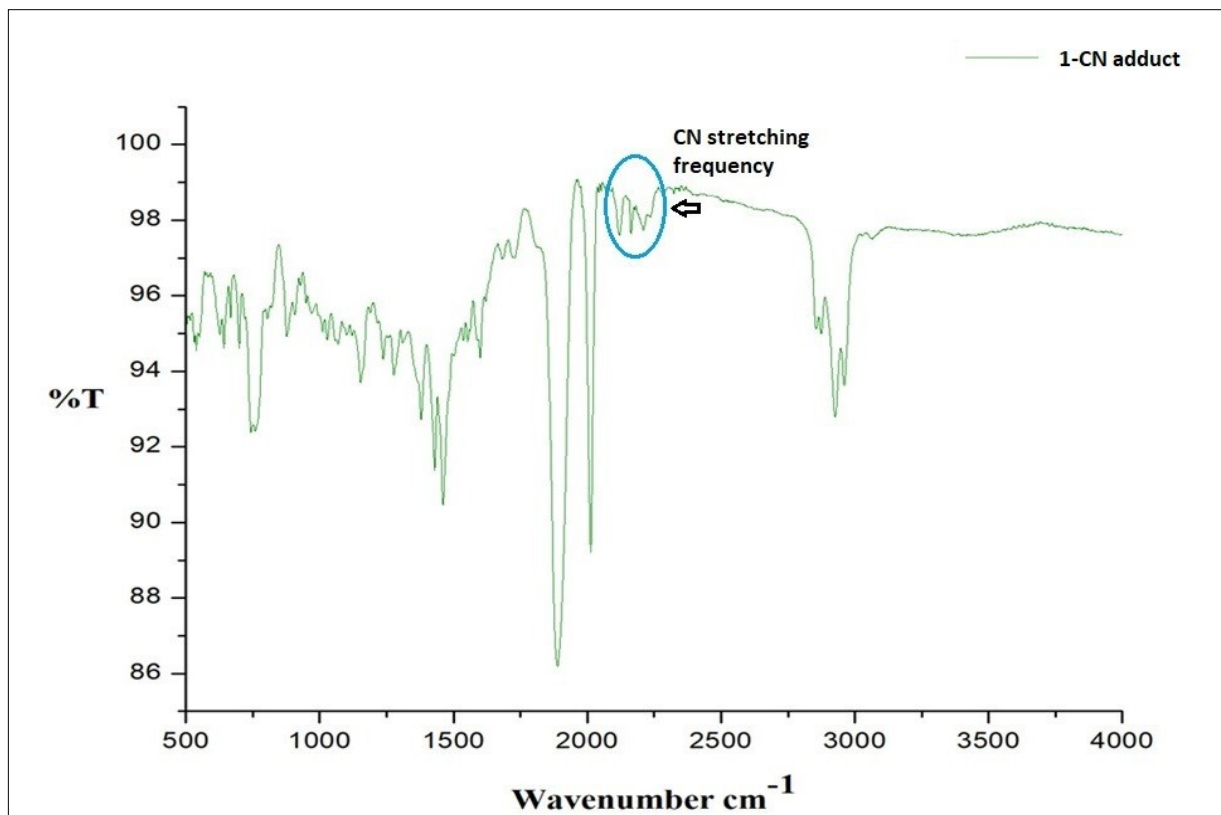


Figure-S13: IR spectra of cyanide adduct

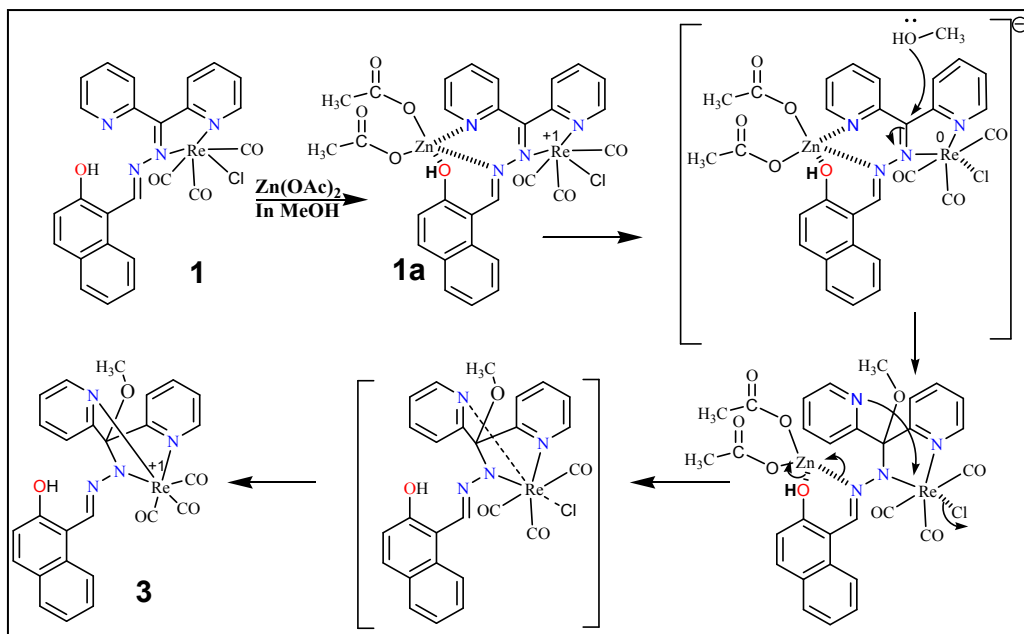


Figure S14: The most probable mechanism for the formation of 3.

In support of the mechanism proposed above, ^1H NMR of **1** is performed in mixed solvent ($\text{CDCl}_3 + \text{CD}_3\text{OD}$) due to low solubility of **1** in CD_3OD . As a result, all the proton signals of **1** are shifted towards downfield region. In fig. 5, the lower most spectra represent proton signals for **1**, where a peak at δ 14.195 shows aldimine proton signal (**a**). The protons adjacent to pyridyl nitrogen (**b** and **c** in fig. 5) shows doublet at δ 13.023 and δ 12.735 respectively. After addition of stoichiometric amount of $\text{Zn}(\text{OAc})_2$ into the solution of **1**, an immediate spectra is recorded. It reveals that, addition of $\text{Zn}(\text{OAc})_2$ causes the proton signals of '**a**', '**b**' and '**c**' to shift more towards downfield region by \sim 0.097 ppm, \sim 0.1 ppm and \sim 0.05 ppm respectively. This observation clearly indicates the interaction of $\text{Zn}(\text{OAc})_2$ with **1**. Here, $\text{Zn}(\text{OAc})_2$ weakly binds with $\text{N}^\wedge\text{N}^\wedge\text{O}$ donor sites of **1**, resulting in the relatively low electron density around aldimine proton and pyridyl protons as $\text{Zn}(\text{II})$ pulls electrons towards itself. This interaction is mainly responsible for the downfield shift of protons.

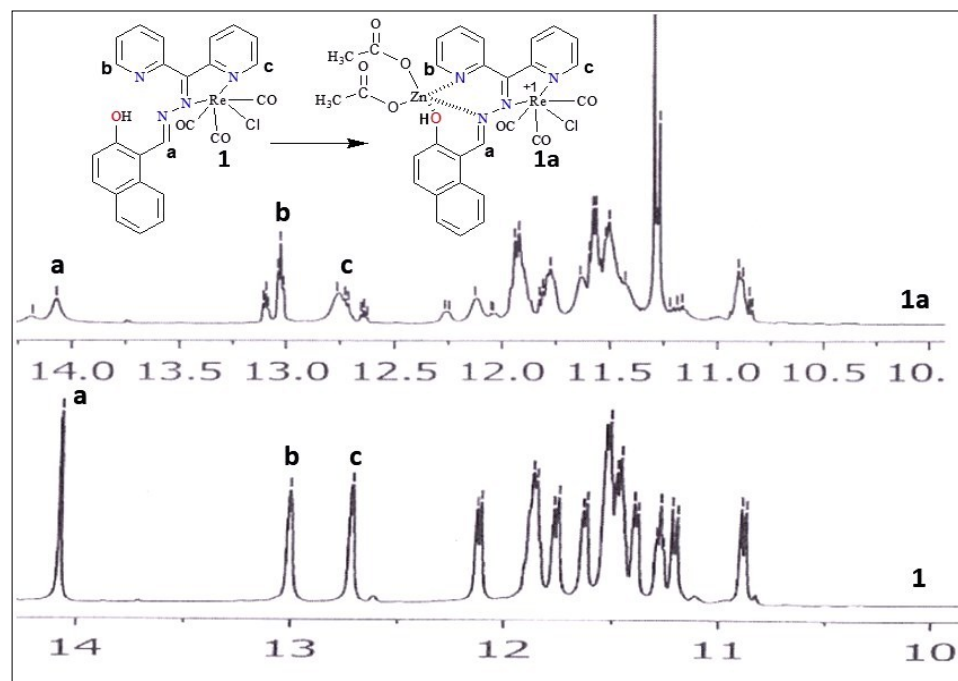


Figure S15: ^1H NMR spectra of **1** (below) and **1a** (above) followed by addition of $\text{Zn}(\text{OAc})_2$. Aldimine proton and protons adjacent to pyridyl moiety are represented by **a**, **b** and **c** respectively.

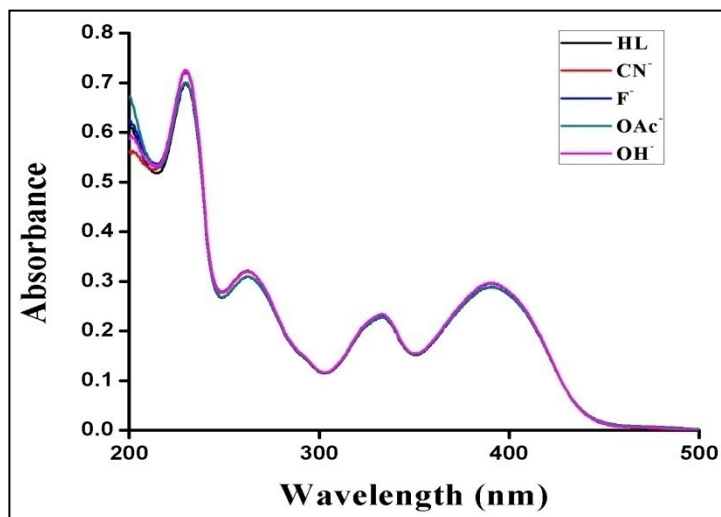


Figure S16: UV-Vis spectra of HL in acetonitrile in presence of various anions.

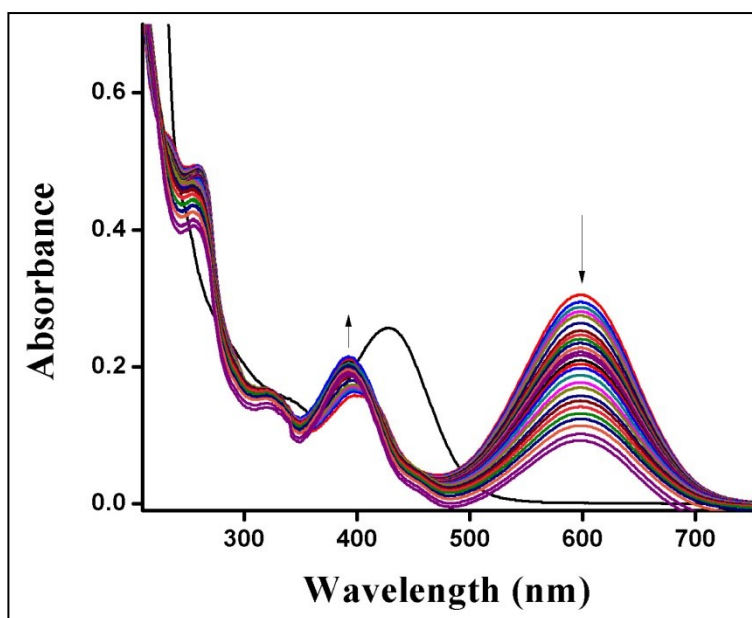


Figure S17: Time evolution UV-Vis spectra (time interval of 5 minutes) of complex **1** ($c = 2 \times 10^{-5}$ M) with 1.5 equivalents of CN^- ion in acetonitrile in presence of F^- , OAc^- , OH^- .

Table S1. Optimized geometrical parameters of 1, 2 and 3

1			2			3		
Bond Length (Å)								
	Exp.	Theo.		Exp.	Theo.		Exp.	Theo.
C1-N1	1.299(7)	1.304	C1-N1	1.403(4)	1.29	C1-N1	1.479(7)	1.47
Re1-C24	1.918(7)	1.926	Re1-O1	2.121(3)	2.15	Re1-C24	1.915(7)	1.93
Re1-C25	1.925(8)	1.929	Re1-C23	1.892(4)	1.91	Re1-C23	1.909(7)	1.91
Re1-C23	2.028(9)	1.913	Re1-C25	1.913(5)	1.92	Re1-C25	1.918(7)	1.92
Re1-N3	2.181(5)	2.208	Re1-C24	1.916(5)	1.93	Re1-N1	2.140(4)	2.18
Re1-N1	2.198(5)	2.221	Re1-N2	2.126(3)	2.16	Re1-N3	2.153(5)	2.20
Re1-Cl1	2.459(2)	2.551	Re1-N4	2.194(4)	2.23	Re1-N4	2.207(5)	2.25
Bond Angles(°)								
C24-Re1-C25	86.0(3)	88.77	C23-Re1-C25	89.47(19)	89.66	C24-Re1-C23	89.2(3)	90.71
C24-Re1-C23	92.2(3)	90.77	C23-Re1-C24	89.3(2)	89.19	C24-Re1-C25	89.3(3)	89.5
C25-Re1-C23	90.6(3)	90.44	C25-Re1-C24	89.6(2)	89.71	C23-Re1-C25	86.8(3)	91.44
C24-Re1-N3	96.3(3)	97.69	C23-Re1-O1	176.14(16)	176.06	C24-Re1-N1	170.0(3)	166.8
C25-Re1-N3	175.3(2)	172.67	C25-Re1-O1	92.34(16)	92.11	C23-Re1-N1	98.2(2)	98.4
C23-Re1-N3	93.4(3)	92.88	C23-Re1-N2	96.93(15)	96.95	C25-Re1-N1	97.8(2)	99.6
C24-Re1-N1	169.8(3)	170.86	C24-Re1-O1	94.13(17)	94.33	C24-Re1-N3	98.1(3)	96.05
C25-Re1-N1	104.2(2)	99.76	C25-Re1-N2	95.06(17)	96.25	C23-Re1-N3	94.4(2)	94.68
C23-Re1-N1	87.5(3)	92.38	C24-Re1-N2	172.24(18)	171.43	C25-Re1-N3	172.5(2)	171.63
N3-Re1-N1	73.59(18)	73.59	O1-Re1-N2	79.52(12)	79.36	N1-Re1-N3	74.70(18)	73.87
C24-Re1-Cl1	93.6(2)	91.50	C23-Re1-N4	92.38(16)	92.70	C24-Re1-N4	97.1(3)	96.25
C25-Re1-Cl1	91.0(2)	91.77	C25-Re1-N4	173.39(17)	173.35	C23-Re1-N4	173.3(2)	172.24
C23-Re1-Cl1	174.0(2)	176.84	C24-Re1-N4	96.75(18)	96.52	C25-Re1-N4	95.4(2)	92.05
N3-Re1-Cl1	84.77(14)	84.65	O1-Re1-N4	85.45(12)	85.15	N1-Re1-N4	75.34(17)	74.07
N1-Re1-Cl1	86.54(14)	85.027	N2-Re1-N4	78.41(13)	77.29	N3-Re1-N4	82.61(18)	81.22
C2-C1-C7	121.0(5)	120.61	C2-C1-C7	117.9(4)	118.04	C2-C1-C7	107.1(5)	105.81

Table S2- Optimized geometries, HOMO and LUMO contour plots of the metal complexes at the B3LYP/6-31G* level

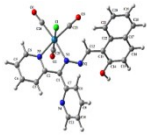
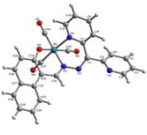
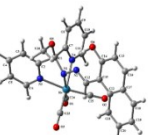
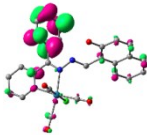
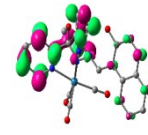
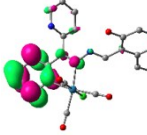
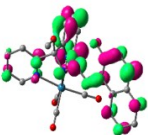
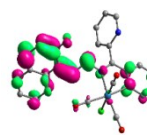
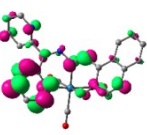
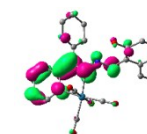
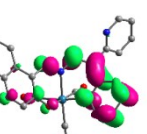
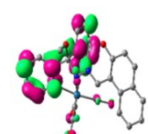
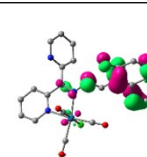
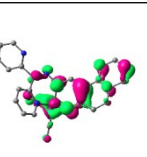
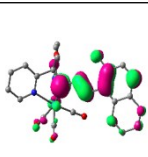
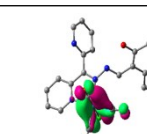
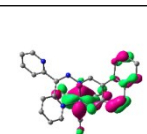
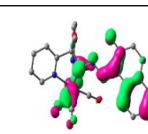
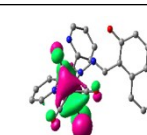
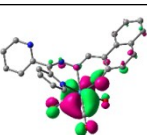
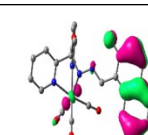
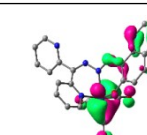
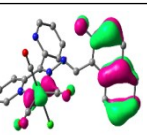
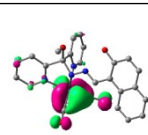
	Complex 1	Complex 2	Complex 3
Optimized geometries at the B3LYP/631G* level			
LUMO+3			
LUMO+2			
LUMO+1			
LUMO			
HOMO			
HOMO-1			
HOMO-2			
HOMO-3			

Table S3: Energies (eV) and composition (%) of frontier molecular orbitals of the complex 1, 2 and 3

Complex-I		% contribution						
MO		CO	Naph	Re	SB	PyA	PyF	Main Bond type
124	L+3	0	6	0	4	42	47	$\pi^*(\text{PyA})+\pi^*(\text{PyF})$
123	L+2	3	0	1	14	50	32	$\pi^*(\text{PyA})+\pi^*(\text{PyF})+\pi(\text{SB})$
122	L+1	3	46	1	27	23	0	$\pi^*(\text{Naph})+\pi^*(\text{PyA})+\pi(\text{SB})$
121	LUMO	1	18	1	37	36	7	$\pi^*(\text{PyA})+\pi^*(\text{Naph})+\pi(\text{SB})$
120	HOMO	9	56	11	25	-4	4	$\pi(\text{Naph})+d(\text{Re})+\pi(\text{SB})$
119	H-1	13	56	26	4	1	0	$\pi(\text{CO})+\pi(\text{Naph})+d(\text{Re})$
118	H-2	27	14	56	1	1	0	$\pi(\text{CO})+\pi(\text{Naph})+d(\text{Re})$
117	H-3	22	22	47	8	1	0	$\pi(\text{CO})+\pi(\text{Naph})+d(\text{Re})$

Complex 2		% Contribution						
MO		CO	Naph	OMe	Re	C=N	Py	Main Bond type
133	L+3	0	16	0	1	4	79	$\pi^*(\text{Naph})+\pi^*(\text{Py})$
132	L+2	2	38	-1	0	15	47	$\pi^*(\text{Naph})+\pi^*(\text{SB})+\pi^*(\text{Py})$
131	L+1	7	16	0	4	7	66	$\pi^*(\text{Naph})+\pi^*(\text{Py})$
130	LUMO	6	1	-1	2	-1	95	$\pi^*(\text{Naph})+\pi^*(\text{Py})$
129	HOMO	5	41	0	4	46	4	$\pi(\text{Naph})+\pi(\text{SB})$
128	H-1	9	55	0	17	17	1	$\pi(\text{Naph})+d(\text{Re})+\pi(\text{SB})$
127	H-2	2	91	0	6	2	0	$\pi(\text{Naph})$
126	H-3	28	0	0	62	1	9	$\pi(\text{CO})+d(\text{Re})$

<i>Complex 3</i>		% Contribution						
MO		CO	Naph	Re	SB	PyA	PyF	Main Bond Type
133	L+3	5	11	3	4	8	68	$\pi^*(\text{Naph}) + \pi^*(\text{PyF})$
132	L+2	2	8	0	7	79	5	$\pi^*(\text{PyA})$
131	L+1	3	50	4	24	19	0	$\pi^*(\text{Naph}) + \pi^*(\text{SB}) + \pi^*(\text{PyA})$
130	LUMO	3	9	2	46	34	5	$\pi^*(\text{SB}) + \pi^*(\text{PyA})$
129	HOMO	2	78	3	14	2	2	$\pi(\text{Naph}) + \pi(\text{SB})$
128	H-1	24	3	48	0	3	0	$\pi(\text{CO}) + d(\text{Re})$
127	H-2	21	3	45	3	2	0	$\pi(\text{CO}) + d(\text{Re})$
126	H-3	6	79	14	1	0	0	$\pi(\text{Naph}) + d(\text{Re})$

Table S4: Natural transition orbitals (NTOs) for the complexes 1–3 illustrating the nature of singlet excited states in the absorption bands. For each state, the respective number of the state, transition energy (eV), and the oscillator strength (in parentheses) are listed. Shown are only occupied (holes) and unoccupied (electrons) NTO pairs that contribute most towards each excited state.

Complex	Transition	Hole	Electron	Assignment
1	S ₃ W=0.97 2.78eV(0.06)			¹ MLCT/ ¹ ILCT
	S ₉ W=0.87 3.81eV(0.02)			¹ MLCT/ ¹ ILCT
	S ₆₈ W= 0.38 5.42eV(0.06)			¹ MLCT/ ¹ ILCT
2	S ₁ W=0.97 2.27eV(0.14)			¹ ILCT/ ¹ MLCT
	S ₄ W=0.92 3.15eV(0.02)			¹ MLCT/ ¹ ILCT
	S ₃₅ W=0.40 4.79eV(0.01)			¹ MLCT/ ¹ ILCT
3	S ₁ W=0.98 2.29eV(0.007)			¹ MLCT/ ¹ ILCT
	S ₄ W=0.76 3.12eV(0.39)			¹ ILCT / ¹ MLCT

Reference for Gaussian 09w Package

M. J. Frisch, G. W. Trucks, H. B. Schlegel, G. E. Scuseria, M. A. Robb, J. R. Cheeseman, G. Scalmani, V. Barone, B. Mennucci, G. A. Petersson, H. Nakatsuji, M. Caricato, X. Li, H. P. Hratchian, A. F. Izmaylov, J. Bloino, G. Zheng, J. L. Sonnenberg, M. Hada, M. Ehara, K. Toyota, R. Fukuda, J. Hasegawa, M. Ishida, T. Nakajima, Y. Honda, O. Kitao, H. Nakai, T. Vreven, J. A. Montgomery Jr., J. E. Peralta, F. Ogliaro, M. Bearpark, J. J. Heyd, E. Brothers, K. N. Kudin, V. N. Staroverov, R. Kobayashi, J. Normand, K. Raghavachari, A. Rendell, J. C. Burant, S. S. Iyengar, J. Tomasi, M. Cossi, N. Rega, J. M. Millam, M. Klene, J. E. Knox, J. B. Cross, V. Bakken, C. Adamo, J. Jaramillo, R. Gomperts, R. E. Stratmann, O. Yazyev, A. J. Austin, R. Cammi, C. Pomelli, J. W. Ochterski, R. L. Martin, K. Morokuma, V. G. Zakrzewski, G. A. Voth, P. Salvador, J. J. Dannenberg, S. Dapprich, A. D. Daniels, Ö. Farkas, J. B. Foresman, J. V. Ortiz, J. Cioslowski and D. J. Fox, **GAUSSIAN 09** (Revision A.1), Gaussian, Inc., Wallingford, CT, **2009**.